Published in final edited form as:

Anal Chem. 2023 July 25; 95(29): 10913–10920. doi:10.1021/acs.analchem.3c00494.

Enhanced Detection of Charged *N*-glycans in the brain by Infrared Matrix-Assisted Laser Desorption Electrospray Ionization Mass Spectrometric Imaging

Juhi Samal[1,*], **Tana V. Palomino**[2,*], **Judy Chen**[1], **David C. Muddiman**[2,**], **Tatiana Segura**[1,**]

[1]Department of Biomedical Engineering, Duke University, Durham, North Carolina State University, Raleigh, NC

[2]Department of Chemistry, North Carolina State University, Raleigh, NC

Abstract

N-linked glycosylation represents a structurally diverse, complex, co- and post-translational protein modification that bridges metabolism and cellular signaling. Consequently, aberrant protein glycosylation is a hallmark of most pathological scenarios. Due to their complex nature and non-template driven synthesis, analysis of glycans is faced with several challenges, underlining the need for new and improved analytical technologies. Spatial profiling of *N*-glycans through direct imaging on tissue sections reveals the regio-specific and/or disease pathology correlating tissue *N*-glycans that serve as a disease glycoprint for diagnosis. Infrared matrix-assisted laser desorption electrospray ionization (IR-MALDESI) is a soft hybrid ionization technique that has been used for diverse mass spectrometry imaging (MSI) applications. Here, we report the first spatial analysis of the brain *N*-linked glycans by IR-MALDESI MSI leading to a significant increase in the detection of the brain *N*-sialoglycans. A formalin-fixed paraffin-embedded mouse brain tissue was analyzed in negative ionization mode after tissue washing, antigen retrieval, and pneumatic application of PNGase F for enzymatic digestion of *N*-linked glycans. We report a comparative analysis of section thickness on the *N*-glycan detection using IR-MALDESI. 136 unique *N*-linked glycans were confidently identified in the brain tissue (with an additional 132 unique *N*-glycans, not reported in GlyConnect), where more than 50% contained sialic acid residues, which is approximately three-fold higher than the previous reports. This work demonstrates the first application of IR-MALDESI in *N*-linked glycan imaging of the brain tissue leading to a 2.5-fold increase in the *in situ* total brain *N*-glycan detection compared to the current gold standard of positive mode matrix-assisted laser desorption/ionization mass spectrometry imaging. This is also the first report of the application of the MSI towards the identification of sulfoglycans in the rodent brain. Overall, IR-MALDESI-MSI presents a sensitive glycan detection platform to identify tissue-specific and/or disease-specific glycosignature in the brain while preserving the sialoglycans without any chemical derivatization.

Graphical Abstract

**Co-corresponding authors.

*These authors contributed equally to this paper

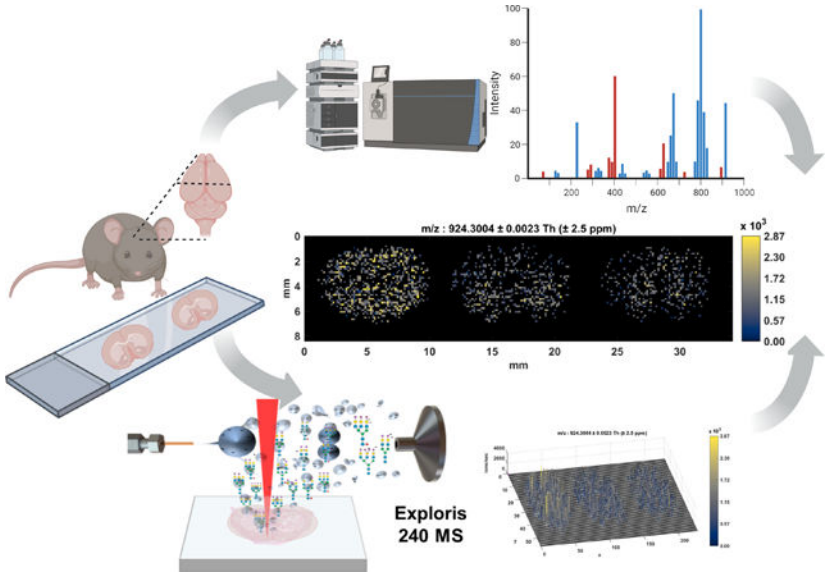

Keywords

IR-MALDESI; *N*-linked glycans; mass spectrometry imaging; brain; sialic acid

INTRODUCTION

Glycosylation is one of the most common post-translational modifications, spanning more than 50% of the eukaryotic proteome[1]. The process of glycosylation involves the enzymatic addition of a glycan moiety (mono-, oligo- or polysaccharides) to a newly-synthesized polypeptide[2]. Unlike, transcription and translation, glycosylation is a non-template driven and dynamic process, which is reflected in the dramatic alteration of the protein glycosylation with the changes within the intra- and extra-cellular milieu. These changes in glycosylation are implicated in regulating the structure and associated function of the proteins. Glycosylation in mammalian glycoproteins is classified into several categories including *N*-linked, *O*-linked, GPI anchored or *O*-GlcNAc modified glycoproteins. Amongst these categories, *N*-linked glycosylation, where the glycan moiety is covalently bound to asparagine residues on proteins containing an N-X-T/S motif where X is any amino acid except proline, covers approximately 90% of eukaryotic glycoproteins[1]. *N*-glycans are ubiquitous in all tissues and are critical in critical biological process such as modulating receptor activation after ligand binding[3] and to mark cell differentiation[4]. In the brain *N*-glycans are implicated in nearly all crucial brain physiological processes like neuronal development and differentiation, synaptogenesis and myelinogenesis[5,6]. However, the impact of the modulation of *N*-linked glycosylation on different aspects of neurological disorders is still unclear partly due to the lack methods to identify the identity and spatial localization of the *N*-glycans. This underlines the need for an in-depth spatial characterization of the brain *N*-glycome of the healthy brains to understand the biological significance of the glycosylation cues and their roles in the region-specific physiological functions and in disease pathophysiology.

Most common analytical platforms for the analysis of brain *N*-linked glycans utilize liquid chromatography-mass spectrometry, wherein there is a loss of spatial resolution and molecular spatial specificity, due to the homogenization of tissue samples during sample preparation for analysis. This necessitates the pre-selection and isolation of the region of interest in order to perform any spatial analysis[7,8]. Mass spectrometric imaging (MSI) of tissue *N*-glycans represents an essential, albeit underexplored, modality for investigating the glycan functions. Contrary to the conventional glycan profiling assays, MSI focuses on the spatial heterogeneity in glycan cues in pathologically or structurally different regions of the tissue.

N-glycans containing negatively charged moieties, such as sialic acid, phosphate, or sulfate groups have been shown to have critical biological implications in the central nervous system[9–11]. Specifically, sialic acids have shown to be involved as key players in the development, plasticity, and repair of the nervous system as well as immune regulation[12]. To date, the MSI of tissue *N*-linked glycans has predominantly used matrix-assisted laser desorption ionization (MALDI), which limits the detection of sialoglycans[13–15]. Some chemical derivatization methods have been developed to circumvent this challenge demanding longer, more complicated sample preparation[16,17]. Electrospray ionization (ESI) based ionization methods overcome other challenges presented by MALDI for the detection of sialoglycans like the higher internal energy deposited by MALDI matrices during proton transfer[18] and the bias of enhanced sialoglycan detection in the negative ionization mode[19]. Infrared matrix-assisted laser desorption electrospray ionization (IR-MALDESI) employs a mid-IR laser to resonantly excite water found in biological specimens[20], desorbing the neutral species into the gas-phase, which are then post-ionized by an orthogonal electrospray plume in an ESI-like fashion prior to analysis by a high resolution, accurate mass Orbitrap mass spectrometer[21]. This hybrid ionization technique harnesses the advantages from both soft ionization sources such as spatial correlation from MALDI and ionization characteristics from ESI, thereby presenting an ideal analytical platform for tissue *N*-glycans. Recent studies from our group have used IR-MALDESI in the direct analysis of native *N*-linked glycans without chemical derivatization[22] and in the mass spectrometric imaging of human prostate tissue for *N*-glycan detection[23].

The current study represents the first application of IR-MALDESI MSI for the detection of brain *N*-linked glycans. The report also presents a comparative analysis of the impact of tissue section thickness on the tissue glycan imaging and detection. To date, there has been no previous reports investigating the detection of tissue glycans as a function of tissue section thickness using MSI. Due to the enhanced sensitivity of IR-MALDESI towards *N*-glycan detection, we report approximately 136 *N*-glycans in the mouse brain. This represents a 2- fold and 3-fold enhanced detection over the previous studies using MALDI MSI, which reported around 55 and 40 mouse brain *N*-glycans respectively[13,15]. To the best of our knowledge, this is the most comprehensive report for spatial resolution of the rodent brain *N*-glycome and identification of charged sialylated and sulfated brain glycans using MSI. This study is of particular significance for future investigation to probe the possible correlation of *N*-glycosylation and its modulation and function in several neurological disorders using IR-MALDESI.

MATERIALS AND METHODS

Sample Preparation

The experiments involving animal use were approved by the Duke Institutional Animal Care and Use Committee (IACUC). C57BL/6 male mice of 8–12 weeks (Jackson Laboratories) were used in the study. Healthy mice were sacrificed with isoflurane and decapitation. The brain was collected immediately after transcardial PBS perfusion, fixed overnight in formalin, and paraffin embedded using standard techniques. Coronal tissue sections of 3, 5 and 7 μm were prepared using a HM 355S rotary microtome (Epredia, Kalamazoo, MI, USA). The sections were mounted onto positively charged slides (Globe Scientific).

Tissue preparation for IR-MALDESI

Mouse brain sections were heated for one hour at 60°C to melt the paraffin around the tissue section. The slides were then cooled to room temperature and deparaffinized and rehydrated using a series of washes as reported previously[23]. After the washes, the slides were dried in a vacuum desiccator for 5 minutes. Antigen retrieval was performed on the dried samples using a vegetable steamer (Rival) which was filled with water and preheated for 5 minutes. Freshly prepared citraconic acid buffer (25 μL of citraconic anhydride, 50 mL of water, and 2 μL of HCl to make pH=3) was used for antigen retrieval process. The slides were placed into a side-opening slide mailer filled with citraconic acid buffer. This slide mailer was then heated in the vegetable steamer for 30 minutes. The mailer was then placed into a container with water to slowly cool down the sample. This was followed by progressive cooling of the samples through buffer exchanges using LC-MS grade water, repeated for a total of three times. The buffer was then fully replaced with water with an additional 5 minutes of cooling, followed by drying in a vacuum-desiccator for 5 minutes.

A TM-Sprayer (HTX Technologies, Carrboro, NC, USA) evenly sprayed the tissue sections with 100 μg/mL of PNGase F PRIME-LY (Bulldog Bio, Portsmouth, NH). The syringe pump was set to 25 μL/min. Nitrogen gas pressure was set to 10 psi and the temperature was adjusted to 45°C. The TM-Sprayer method was set to 15 passes, 1200 mm/min velocity, 3 mm track spacing, 5 mm overspray margins using the crisscross pattern. Sprayed slides were incubated in a controlled humidity chamber at 37°C for 2 hours and the relative humidity was monitored to be around 95% during incubation.

IR-MALDESI Data Collection

Mouse brain slides were individually placed onto a Peltier-cooled stage inside of a humidity chamber. The chamber was purged with nitrogen gas (Arc3 Gases, Raleigh NC, USA) and the stage was cooled to −8°C. A thin ice layer was formed over the glass slide by controlling the humidity, whichserved as the ice matrix. The relative humidity was lowered to < 12% for the imaging experiment. The electrospray solution was composed of 50% acetonitrile with 1 mM acetic acid (Fischer Scientific, Nazareth, PA, USA). A corresponding flow rate of 1 μL/min and a voltage of 3000V was used to create an electrospray plume in negative ionization mode. The laser source (JGMA, Burlington, MA, USA) was a mid-IR laser that fired 10 pulses per burst at a wavelength of 2970 nm. Ablation consisted of 1 mJ of energy per voxel and a spatial resolution of 150 μm. An Orbitrap Exploris 240 mass spectrometer

(Thermo Fisher Scientific, Bremen, Germany) was used for data collection within a range of 500 to 2000 m/z. The instrument was mass calibrated every day of analysis in order to achieve high mass measurement accuracy. Automatic gain control was disabled and the injection time was fixed at 90 ms.

Data Analysis

Raw data files were converted to imzML files using MSConvert[24] and imzML converter[25]. Files were uploaded into MSiReader for analyzing the MSI data[26,27]. All ion images were created and analyzed using MSiReader. The data was searched for multiply-charged ions, and *m/z* values were converted to monoisotopic mass. Glycomod, a theoretical glycan mass database, was used to search the data for any matches using accurate mass. The glycan compositions reported in the current study were detected as confident identifications on GlyConnect, an experimentally curated glycomic database[28].The results were filtered to be within a 5 ppm mass tolerance, containing the *N*-linked glycan core and excluding pentose, KDN, and HexA. GlyConnect, an experimental database, was used to confirm *N*-linked glycan mass and structure.

Statistical analysis

All results will be representative of those from at least three independent experiments with similar observations. For two-sample comparison, Student's t-test was performed. For multiple-sample comparisons, one-way or two-way analysis of variance (ANOVA) was performed, followed by a post hoc multiple comparison procedure (Dunn or Tukey). Two-way ANOVA was used for the experiments performed over time. The comparison results are presented with raw and false discovery rate (FDR) adjusted p-values at the alpha 0.05 level of significance. To reduce bias in sample selection, randomized experimental design was used.

RESULTS AND DISCUSSION

IR-MALDESI coupled to an Orbitrap enables high spatial and mass spectral resolution for both neutral and charged *N*-glycans by combining MALDI and ESI characteristics of spatial correlation and soft ionization to enable the identification of labile glycan moieties *in situ*. Given these advantages, the current study was designed to evaluate the performance of IR-MALDESI platform on the *in situ* brain *N*-glycan imaging analysis.

In this study, we adapted the previously optimized IR-MALDESI platform[23] and successfully applied it to the imaging and identification of multiple sialylated *N*-linked glycans in the brain, without prior derivatization, for the first time. Figure 1 shows the sample preparation workflow used for the preparation of the brain samples for the N-glycan release and in situ detection by IR-MALDESI analyses. The first step involves heating the sample slide at 60^{o}C for an hour followed by several solvent washes in xylenes and ethanol, followed by rinsing in water to remove paraffin, salts, and metabolites from the FFPE processed tissue sections[29]. Heating the samples facilitates protein denaturation on the tissue sections to better expose the glycoproteins for glycan release and detection. This step also removes some lipids, which is crucial for brain *N*-glycan imaging as the

lipids constitute more than 50% of the dry weight of the brain[30]. The higher lipid fraction would obscure the glycan signal detection in the recorded mass spectra, which necessitates the initial tissue delipidation during the dewaxing step. Antigen retrieval using citraconic buffer was performed to allow the enzyme to access to the glycosylation sites in the cross-linked proteins. Finally, PNGase F was pneumatically sprayed over the brain sections to maximize the tissue coverage and enzyme utilization ratio for optimal release of the tissue *N*-glycans. Released *N*-linked glycans were then analyzed by IR-MALDESI in negative ionization mode which facilitated higher and more sensitive detection of the negatively charged sialylated species[22].

Glycans present on the cell surface and extracellular matrix of the brain play a crucial role in the maintenance of brain homeostasis[31]. Protein *N*-glycosylation, where the glycans are covalently attached to an asparagine by an *N*-glycosidic bond, comprises of the most predominant type of protein glycosylation in the eukaryotic cells[1]. There have been previous studies investigating the role and modulation of *N*-glycosylation in neurological disorders like Alzheimer's Disease[32] and Parkinson's disease[33] and most of the proteins associated with these disease pathophysiology are glycosylated[34]. This commands the development of a comprehensive glycan map of the brain correlating the glycans to different functional regions in the brain. The structure-function correlation would lead to a better understanding of the roles of glycans as well as provide potential therapeutic targets for neurological disorders. Imaging mass spectrometric analysis of glycans reveals the spatial resolution of glycans detected in tissue specimens, which is lost in other bulk mass spectrometric methods like LC-MS analysis.

We tested the applicability of the IR-MALDESI platform for high-resolution glycan MSI analysis of mouse brain. Combining the advantages of MALDI and ESI strategies, we were able to detect a total of 136 multiply-charged deprotonated *N*-linked glycans using IR-MALDESI with high mass measurement accuracy (MMA, <5 ppm) in the mouse brain sample. We have reported the 50 highest ion abundance brain glycans with their compositions in Table 1 and a detailed list of all the *N*-glycans identified is presented in Supplementary Table S1. Figure S1 presents the panel of ion images showing spatial resolution for the *N*-glycans as reported in Table 1, with the corresponding glycan structures. This demonstrates approximately a 2.5-fold increase in the number of glycans detected by Shi *et al.* using Sub-AP/MALDI MSI[13] and 3-fold increase over those detected by Eshghi *et al.* using MALDI-MSI[15] (Figure 2a,b). Approximately 70% of the new glycans detected in the current study were found to be sialylated with at least one sialic acid derivative (Table S2).

We also performed a comparative analysis of different tissue section thicknesses (3, 5 and 7 μm) and their impact on the *N*-glycan detection using IR-MALDESI. To the best of our knowledge, this is the first analysis of the impact of section thickness on the *N*-glycan detection using MSI. Filtered peaks were cross-referenced in GlyConnect and the *N*-Linked containing minimum three hexose and two *N*-acetylglucosamines (core pentasaccharide structure) with the monoisotopic peaks of the second or third charge state overlapping the experimental mass range were reported for all three section thicknesses (Figure 2c). Although there aren't significant differences between the glycan compositions reported

between different section thicknesses, 3 μm section thickness shows a higher ion abundance for the same glycan as compared to 5 μm and 7 μm sections (Figure 2D). This could be attributed to the more efficient, complete *in situ* enzymatic digestion in thinner tissue section. Previous MSI brain glycan studies in mouse brain have used section thicknesses ranging from 6–10 μm for both fresh frozen and FFPE processed tissues[13,14,35]. Due to the ease of tissue sectioning and no significant difference in glycan detection at 5 μm, we used 5 μm section thickness for subsequent analysis. The unique glycan compositions detected in 3 and 7 μm sections have been reported in Table S4 and S5 respectively.

Pace *et al.*[23] reported the presence of several chlorinated adducts using the mixed-mode ionization in IR-MALDESI in the human prostate tissue. This led to the annotation of additional *N*-linked glycan peaks that were previously unidentified. Consistent with these observations, we detected multiple chlorinated adducts in the current study. The isotopic distributions of the detected *N*-linked glycans aligned well with the theoretical distribution of the glycans with chlorinated adducts as represented in Figure 3B and 3C. Figure 3B shows that $Hex_7HexNAc_6Fuc_1NeuAc_1$ is detected as a chlorine adduct with one chlorine derivative and the loss of a proton and Figure 3C represents $Hex_4HexNAc_5Fuc_2$ detected with two chlorine adducts. The experimental data aligns very closely with the theoretical isotopic distribution as demonstrated by the chi-squared value, evaluating the goodness of fit between two distributions. This result validates the detection of several brain *N*-glycans using IR-MALDESI as chlorinated adducts in the negative ionization mode.

Previous studies have shown a spatio-specific regulation of N-glycosylation in rodent brain, which is further modulated in pathophysiological conditions[8,13–15,36]. Sensitive spatial resolution of *N*-glycans, is therefore, very consequential towards the identification of glycan cues implicated in disease pathology. Therefore, we investigated the applicability of the IR-MALDESI platform for high resolution *N*-glycan mass spectrometric imaging of FFPE mouse brain. Using this platform, 136 *N*-glycans including high-mannose, complex and hybrid glycans were detected and annotated by the accurate mass matching using GlyConnect (Figure 4a and Table S1). Figure 4a shows the glycans that were identified using GlyConnect with the structural annotations in the *m/z* range of 900–1250. The spectra also shows other multiply charged, possible *N*-glycan peaks in this region, which have not been reported in GlyConnect. Table S3 reports all the glycan compositions that were identified in the spectra, but were not reported in GlyConnect and Figure S2 shows the representative ion images for some of these glycans. The lack of multiply-charged peaks in the IR-MALDESI background spectra (*i.e.*, off tissue) indicate that these peaks can be attributed to *N*-linked glycans. These multiply-charged peaks were searched in GlycoMod for theoretical identifications and resulted in further detection of 132 unique *N*-glycans after deisotoping and verifying the detection of the isotopic distribution.

Several studies have highlighted the significance of the sialic acids in immune and nervous system regulation. Dysregulated sialylation has been shown to contribute to several chronic diseases of the central nervous system (CNS)[37,38]. This underlines the need for technology development for sensitive detection of tissue *N*-sialoglycans to detect the expression and modulation of sialic acids in the disease pathophysiology towards the development of therapeutic interventions. The increased sensitivity of IR-MALDESI platform towards the

detection of multiply-charged glycans compared to previous reports, resulted in the detection of significantly higher number of sialylated glycans in the mouse brain using different MSI platforms. More than 50% of the total *N*-glycans detected were found to be sialylated (Table S1) and of all the unreported glycans from the imaging mass spectrometric studies 70.68% were sialylated (Table S2). This is approximately 3-fold higher than the sialylated glycans (~13%) detected by Shi *et al*[13]. The enhanced detection multiply-charged sialylated *N*-glycans, which are otherwise labile and difficult to detect using MALDI, is attributed to the 'soft' ionization harnessed in the IR-MALDESI[39]. The differential distribution of glycans in the mouse brain was detected in this analysis and the representative images are shown in Figure 4b–f. These results signify the adaptability of the IR-MALDESI platform for sensitive *N*-glycan detection and visualization from FFPE brain sections for charged and neutral *N*-glycans without any further derivatization. This alleviates the need for additional sample processing and loss of glycans in the additional processing steps.

Using IR-MALDESI platform, we were able to detect oligomannose, hybrid and complex glycans (Figure 5a). Spatial resolution of the representative glycans from each of these classes is represented in Figure 5c–e. A higher fraction of fucosylated glycans were detected in the brain which aligns with the previous reports [7,8]. In the current study, we were able to detect multiple sialic acid and fucose (mono-, di-, tri- and tetra-) substitutions as represented in Figure S3.

Sulfated *N*- and *O*-glycan epitopes are known to be implicated in mediating a diverse range of biological recognition functions and pathophysiological implications [40–42]. However, the detection of these low abundance and crucial sulfated glycans has necessitated the development of new enrichment strategies and methods directed at sulfoglycomics[43,44]. To the best of our knowledge, this is the first glycan MSI analysis to report these *N*-sulfoglycans in the brain tissue analysis. Further, the ambient, *in situ* analysis conditions bypass the need for chemical modifications to stabilize and detect the sulfated glycans. The sulfated glycans were detected as multiply-charged species (Figure 6). Interestingly, the spatial distribution of the representative sulfated glycans shows a higher density of these sulfated *N*-glycans around the corpus callosum, which is characterized by the presence of a cluster of myelinated nerve fibers[45]. Sulfated *N*-glycans have been shown to be implicated in the peripheral nervous system myelination[46]. Myelination is implicated in tuning axonal functions and degeneration of demyelinated axons mediates permanent neurological disability[47,48]. The spatial localization of the sulfated glycans in the myelin-enriched corpus callosum in the brain underlines the significance of the spatial glycan cues in disease pathophysiology in several myelin disorders.

CONCLUSIONS

We report a charged glycan sensitive MSI strategy to spatially resolve the *N*-linked glycans in the brain. A total of 136 *N*-linked glycans were confidently identified based on previous identifications found in the literature. We also report around 50% sialoglycans in the total glycans detected, which is 3-fold higher than the previous reports. The study reports a significant amount of multiply-charged peaks, identifying potential sulfate modifications in the brain as well as several chlorine-adducted structures. This report demonstrates a

sensitive, sialoglycan preserving, *in situ N*-linked glycan imaging by IR-MALDESI for brain tissue, alleviating the need for chemical derivatization. This study reports a reproducible spatial profiling platform for the brain glycome to serve as a baseline for the identification of glycan biomarkers and their regulation in acute and chronic brain disorders.

Supplementary Material

Refer to Web version on PubMed Central for supplementary material.

ACKNOWLEDGEMENTS

The authors gratefully acknowledge the financial support received from the National Institutes of Health (R01GM087964 and 2R01NS079691). All the animal experiments and tissue processing was performed at Duke University and the glycan mass spectrometric imaging was performed in the Molecular Education, Technology and Research Innovation Center (METRIC) at North Carolina State University. The graphical abstract and protocol schematic was created using BioRender with publication license.

REFERENCES

1. Apweiler R, Hermjakob H & Sharon N On the frequency of protein glycosylation, as deduced from analysis of the SWISS-PROT database11Dedicated to Prof. Akira Kobata and Prof. Harry Schachter on the occasion of their 65th birthdays. Biochimica et Biophysica Acta (BBA) - General Subjects 1473, 4–8 (1999). 10.1016/S0304-4165(99)00165-8 [PubMed: 10580125]
2. Hart GW & Copeland RJ Glycomics hits the big time. Cell 143, 672–676 (2010). 10.1016/j.cell.2010.11.008 [PubMed: 21111227]
3. Chandler KB et al. N-Glycosylation regulates ligand-dependent activation and signaling of vascular endothelial growth factor receptor 2 (VEGFR2). Journal of Biological Chemistry 294, 13117–13130 (2019). 10.1074/jbc.RA119.008643 [PubMed: 31308178]
4. Link-Lenczowski P et al. A switch of N-glycosylation of proteome and secretome during differentiation of intestinal epithelial cells. Biochimica et Biophysica Acta (BBA) - Molecular Cell Research 1866, 118555 (2019). 10.1016/j.bbamcr.2019.118555 [PubMed: 31499077]
5. Conroy LR, Hawkinson TR, Young LEA, Gentry MS & Sun RC Emerging roles of N-linked glycosylation in brain physiology and disorders. Trends in Endocrinology & Metabolism 32, 980–993 (2021). 10.1016/j.tem.2021.09.006 [PubMed: 34756776]
6. Scott H & Panin VM N-glycosylation in regulation of the nervous system. Adv Neurobiol 9, 367–394 (2014). 10.1007/978-1-4939-1154-7_17 [PubMed: 25151388]
7. Ji IJ et al. Spatially-Resolved Exploration of the Mouse Brain Glycome by Tissue Glyco-Capture (TGC) and Nano-LC/MS. Analytical Chemistry 87, 2869–2877 (2015). 10.1021/ac504339t [PubMed: 25643168]
8. Samal J, Saldova R, Rudd PM, Pandit A & O'Flaherty R Region-Specific Characterization of N-Glycans in the Striatum and Substantia Nigra of an Adult Rodent Brain. Analytical Chemistry 92, 12842–12851 (2020). 10.1021/acs.analchem.0c01206 [PubMed: 32815717]
9. Kadomatsu K & Sakamoto K Sulfated glycans in network rewiring and plasticity after neuronal injuries. Neuroscience Research 78, 50–54 (2014). 10.1016/j.neures.2013.10.005 [PubMed: 24157431]
10. Silverman-Gavrila LB, Senzel AG, Charlton MP & Feng ZP Expression, phosphorylation, and glycosylation of CNS proteins in aversive operant conditioning associated memory in Lymnaea stagnalis. Neuroscience 186, 94–109 (2011). 10.1016/j.neuroscience.2011.04.027 [PubMed: 21530618]
11. Schnaar RL, Gerardy-Schahn R & Hildebrandt H Sialic acids in the brain: gangliosides and polysialic acid in nervous system development, stability, disease, and regeneration. Physiol Rev 94, 461–518 (2014). 10.1152/physrev.00033.2013 [PubMed: 24692354]

12. Lünemann JD, von Gunten S & Neumann H Targeting sialylation to treat central nervous system diseases. Trends in Pharmacological Sciences 42, 998–1008 (2021). 10.1016/j.tips.2021.09.002 [PubMed: 34607695]
13. Shi Y et al. Mass Spectrometry Imaging of N-Glycans from Formalin-Fixed Paraffin-Embedded Tissue Sections Using a Novel Subatmospheric Pressure Ionization Source. Analytical Chemistry 91, 12942–12947 (2019). 10.1021/acs.analchem.9b02995 [PubMed: 31507162]
14. Powers TW et al. Matrix Assisted Laser Desorption Ionization Imaging Mass Spectrometry Workflow for Spatial Profiling Analysis of N-Linked Glycan Expression in Tissues. Analytical Chemistry 85, 9799–9806 (2013). 10.1021/ac402108x [PubMed: 24050758]
15. Toghi Eshghi S et al. Imaging of N-Linked Glycans from Formalin-Fixed Paraffin-Embedded Tissue Sections Using MALDI Mass Spectrometry. ACS Chemical Biology 9, 2149–2156 (2014). 10.1021/cb500405h [PubMed: 25029481]
16. Grzeski M et al. In Situ N-Glycosylation Signatures of Epithelial Ovarian Cancer Tissue as Defined by MALDI Mass Spectrometry Imaging. Cancers 14, 1021 (2022). [PubMed: 35205768]
17. Holst S et al. Linkage-Specific in Situ Sialic Acid Derivatization for N-Glycan Mass Spectrometry Imaging of Formalin-Fixed Paraffin-Embedded Tissues. Analytical Chemistry 88, 5904–5913 (2016). 10.1021/acs.analchem.6b00819 [PubMed: 27145236]
18. Harvey DJ Structural determination of N-linked glycans by matrix-assisted laser desorption/ ionization and electrospray ionization mass spectrometry. Proteomics 5, 1774–1786 (2005). 10.1002/pmic.200401248 [PubMed: 15832364]
19. Powell AK & Harvey DJ Stabilization of sialic acids in N-linked oligosaccharides and gangliosides for analysis by positive ion matrix-assisted laser desorption/ionization mass spectrometry. Rapid Commun Mass Spectrom 10, 1027–1032 (1996). 10.1002/(sici)1097-0231(19960715)10:9<1027::Aid-rcm634>3.0.Co;2-y [PubMed: 8755235]
20. Robichaud G, Barry JA & Muddiman DC IR-MALDESI mass spectrometry imaging of biological tissue sections using ice as a matrix. J Am Soc Mass Spectrom 25, 319–328 (2014). 10.1007/s13361-013-0787-6 [PubMed: 24385399]
21. Caleb Bagley M, Garrard KP & Muddiman DC The development and application of matrix assisted laser desorption electrospray ionization: The teenage years. Mass Spectrom Rev (2021). 10.1002/mas.21696
22. Pace CL & Muddiman DC Direct Analysis of Native N-Linked Glycans by IR-MALDESI. Journal of the American Society for Mass Spectrometry 31, 1759–1762 (2020). 10.1021/jasms.0c00176
23. Pace CL, Angel PM, Drake RR & Muddiman DC Mass Spectrometry Imaging of N-Linked Glycans in a Formalin-Fixed Paraffin-Embedded Human Prostate by Infrared Matrix-Assisted Laser Desorption Electrospray Ionization. Journal of Proteome Research 21, 243–249 (2022). 10.1021/acs.jproteome.1c00822 [PubMed: 34860526]
24. Kessner D, Chambers M, Burke R, Agus D & Mallick P ProteoWizard: open source software for rapid proteomics tools development. Bioinformatics 24, 2534–2536 (2008). 10.1093/bioinformatics/btn323 [PubMed: 18606607]
25. Race AM, Styles IB & Bunch J Inclusive sharing of mass spectrometry imaging data requires a converter for all. J Proteomics 75, 5111–5112 (2012). 10.1016/j.jprot.2012.05.035 [PubMed: 22641155]
26. Bokhart MT, Nazari M, Garrard KP & Muddiman DC MSiReader v1.0: Evolving Open-Source Mass Spectrometry Imaging Software for Targeted and Untargeted Analyses. Journal of the American Society for Mass Spectrometry 29, 8–16 (2018). 10.1007/s13361-017-1809-6 [PubMed: 28932998]
27. Robichaud G, Garrard KP, Barry JA & Muddiman DC MSiReader: An Open-Source Interface to View and Analyze High Resolving Power MS Imaging Files on Matlab Platform. Journal of the American Society for Mass Spectrometry 24, 718–721 (2013). 10.1007/s13361-013-0607-z [PubMed: 23536269]
28. Mariethoz J et al. Glycomics@ExPASy: Bridging the Gap. Mol Cell Proteomics 17, 2164–2176 (2018). 10.1074/mcp.RA118.000799 [PubMed: 30097532]

29. Yang J & Caprioli RM Matrix Sublimation/Recrystallization for Imaging Proteins by Mass Spectrometry at High Spatial Resolution. Analytical Chemistry 83, 5728–5734 (2011). 10.1021/ac200998a [PubMed: 21639088]
30. Hamilton JA, Hillard CJ, Spector AA & Watkins PA Brain Uptake and Utilization of Fatty Acids, Lipids and Lipoproteins: Application to Neurological Disorders. Journal of Molecular Neuroscience 33, 2–11 (2007). 10.1007/s12031-007-0060-1 [PubMed: 17901539]
31. Zhao F, Zhong L & Luo Y Endothelial glycocalyx as an important factor in composition of blood-brain barrier. CNS Neuroscience & Therapeutics 27, 26–35 (2021). 10.1111/cns.13560 [PubMed: 33377610]
32. Frenkel-Pinter M et al. Interplay between protein glycosylation pathways in Alzheimer's disease. Science Advances 3, e1601576 (2017). 10.1126/sciadv.1601576 [PubMed: 28929132]
33. Raghunathan R, Hogan JD, Labadorf A, Myers RH & Zaia J A glycomics and proteomics study of aging and Parkinson's disease in human brain. Scientific Reports 10, 12804 (2020). 10.1038/s41598-020-69480-3 [PubMed: 32733076]
34. Haukedal H & Freude KK Implications of Glycosylation in Alzheimer's Disease. Frontiers in Neuroscience 14 (2021). 10.3389/fnins.2020.625348
35. Fülöp A et al. Device-Controlled Microcondensation for Spatially Confined On-Tissue Digests in MALDI Imaging of N-Glycans. Pharmaceuticals 15, 1356 (2022). [PubMed: 36355528]
36. Rebelo AL et al. Complete spatial characterisation of N-glycosylation upon striatal neuroinflammation in the rodent brain. Journal of Neuroinflammation 18, 116 (2021). 10.1186/s12974-021-02163-6 [PubMed: 33993882]
37. Boligan KF, Mesa C, Fernandez LE & von Gunten S Cancer intelligence acquired (CIA): tumor glycosylation and sialylation codes dismantling antitumor defense. Cellular and Molecular Life Sciences 72, 1231–1248 (2015). 10.1007/s00018-014-1799-5 [PubMed: 25487607]
38. Rawal P & Zhao L Sialometabolism in Brain Health and Alzheimer's Disease. Front Neurosci 15, 648617 (2021). 10.3389/fnins.2021.648617 [PubMed: 33867926]
39. Tu A & Muddiman DC Internal Energy Deposition in Infrared Matrix-Assisted Laser Desorption Electrospray Ionization With and Without the Use of Ice as a Matrix. Journal of the American Society for Mass Spectrometry 30, 2380–2391 (2019). 10.1007/s13361-019-02323-2 [PubMed: 31502226]
40. Xiong L, Andrews D & Regnier F Comparative Proteomics of Glycoproteins Based on Lectin Selection and Isotope Coding. Journal of Proteome Research 2, 618–625 (2003). 10.1021/pr0340274 [PubMed: 14692455]
41. Chance DL & Mawhinney TP Disulfated oligosaccharides derived from tracheobronchial mucous glycoproteins of a patient suffering from cystic fibrosis. Carbohydrate Research 295, 157–177 (1996). 10.1016/S0008-6215(96)90136-6 [PubMed: 9002191]
42. Fukuda M, Hiraoka N, Akama TO & Fukuda MN Carbohydrate-modifying Sulfotransferases: Structure, Function, and Pathophysiology*. Journal of Biological Chemistry 276, 47747–47750 (2001). 10.1074/jbc.R100049200 [PubMed: 11585845]
43. Yu S-Y, Wu S-W, Hsiao H-H & Khoo K-H Enabling techniques and strategic workflow for sulfoglycomics based on mass spectrometry mapping and sequencing of permethylated sulfated glycans. Glycobiology 19, 1136–1149 (2009). 10.1093/glycob/cwp113 [PubMed: 19671626]
44. Lei M, Mechref Y & Novotny MV Structural Analysis of Sulfated Glycans by Sequential Double-Permethylation Using Methyl Iodide and Deuteromethyl Iodide. Journal of the American Society for Mass Spectrometry 20, 1660–1671 (2009). 10.1016/j.jasms.2009.05.001 [PubMed: 19546010]
45. Harker A in The Neurobiology of Brain and Behavioral Development (eds Robbin Gibb& Bryan Kolb) 439–467 (Academic Press, 2018).
46. Yoshimura T et al. GlcNAc6ST-1 regulates sulfation of N-glycans and myelination in the peripheral nervous system. Scientific Reports 7, 42257 (2017). 10.1038/srep42257 [PubMed: 28186137]
47. Nave KA & Trapp BD Axon-glial signaling and the glial support of axon function. Annu Rev Neurosci 31, 535–561 (2008). 10.1146/annurev.neuro.30.051606.094309 [PubMed: 18558866]
48. Quarles RH Comparison of CNS and PNS myelin proteins in the pathology of myelin disorders. J Neurol Sci 228, 187–189 (2005). 10.1016/j.jns.2004.10.005

Synopsis:

A soft ionization based mass spectrometric imaging modality that preservers and significantly enhances charged (3-fold increase) *N*-glycan detection in the mouse brain without chemical derivatization.

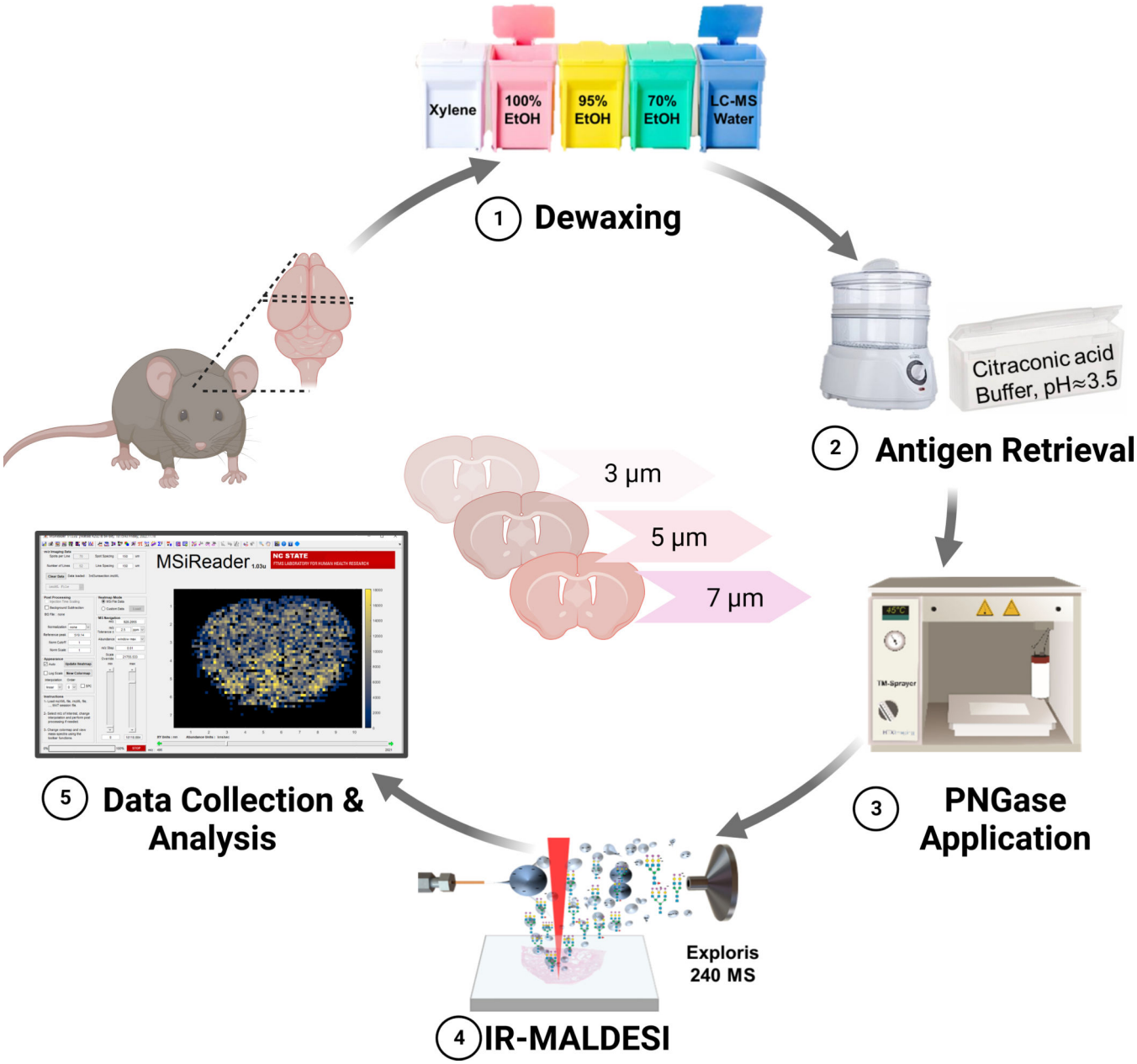

Figure 1:
Schematic outline of the sample preparation, test conditions and IR-MALDESI analysis of FFPE mouse brain sections of 8-week old C57BL6 mouse

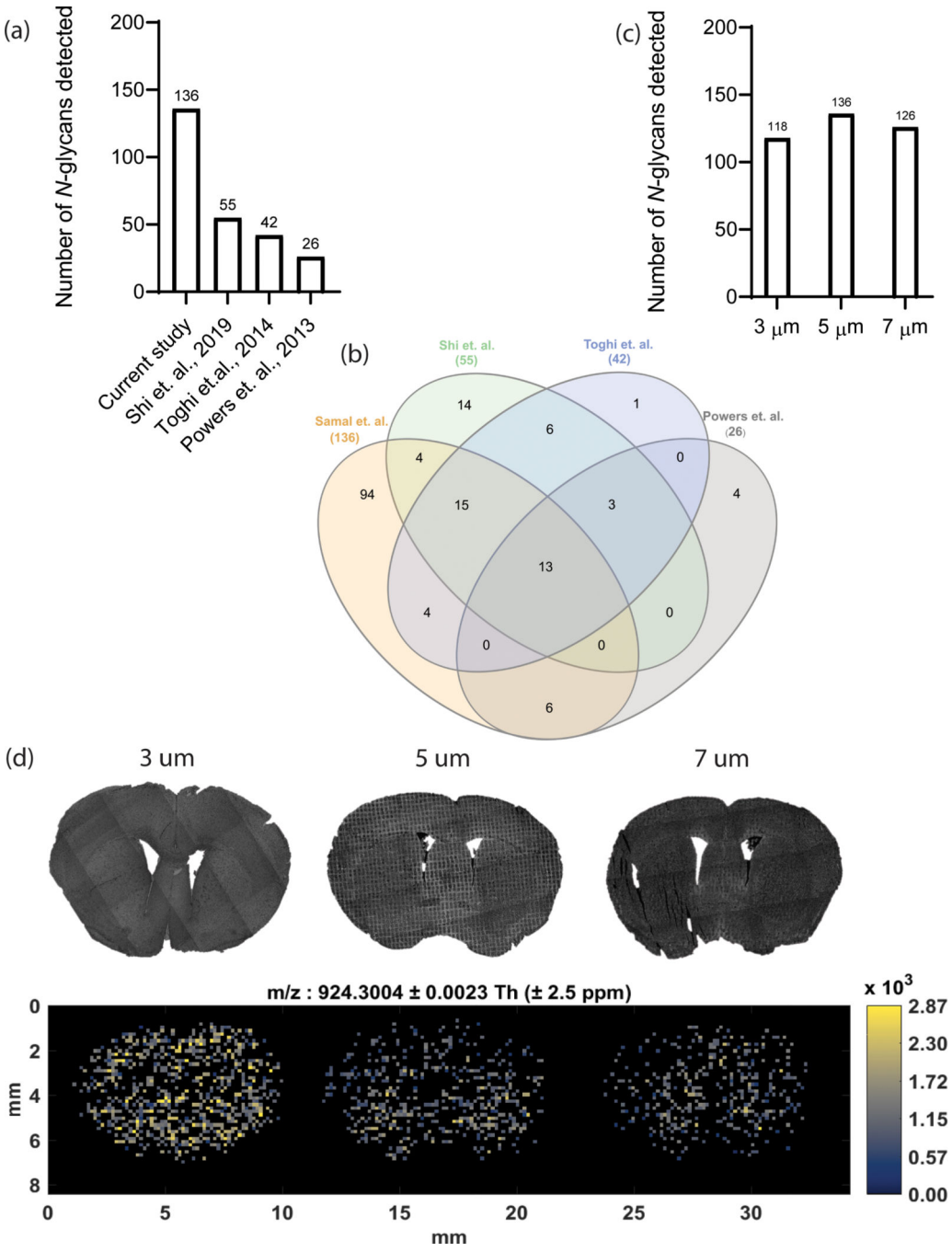

Figure 2:

Increased glycan detection as a function of tissue section thickness analysis **(a)** Approximately 3-fold increase in *N*-glycan detection from FFPE mouse brain tissue section by using the novel IR-MALDESI platform. **(b)** Venn diagram showing the overlap of *N*-glycans detected in the current study with *N*-glycans reported in prior investigations[13–15] using MALDI-MS platform. **(c)** No significant changes in the *N*-glycan detection with different section thicknesses and **(d)** MS images of a representative *N*-glycan showing the

impact of section thickness on *N*-glycan detection. 3 μm section thickness shows a more abundant detection as compared to the 5 and 7 μm sections

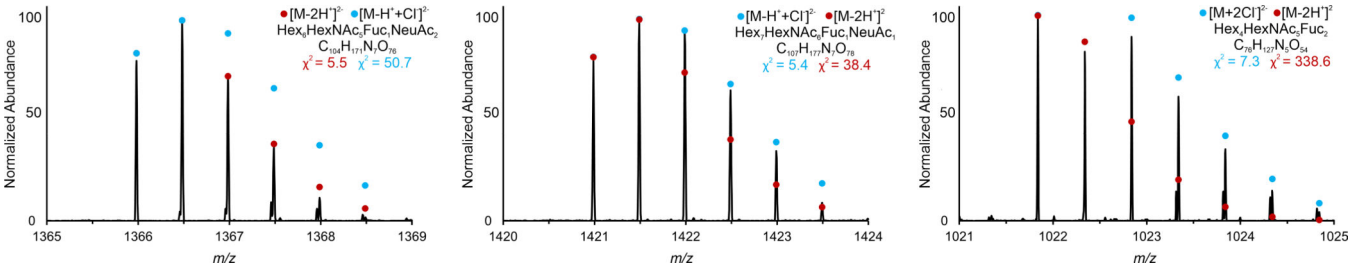

Figure 3: Chlorinated adducts of *N*-glycans detected in the brain:

(A, B, C) Isotopic distributions of three detected *N*-linked glycans with theoretical distributions of chlorine and deprotonated adducts overlaid. Chi-squared values testing a goodness of fit confirm the detection of *N*-linked glycans with single and double chlorine adducts, confirming the detection of chlorinated adducts in the negative ionization mode using IR-MALDESI

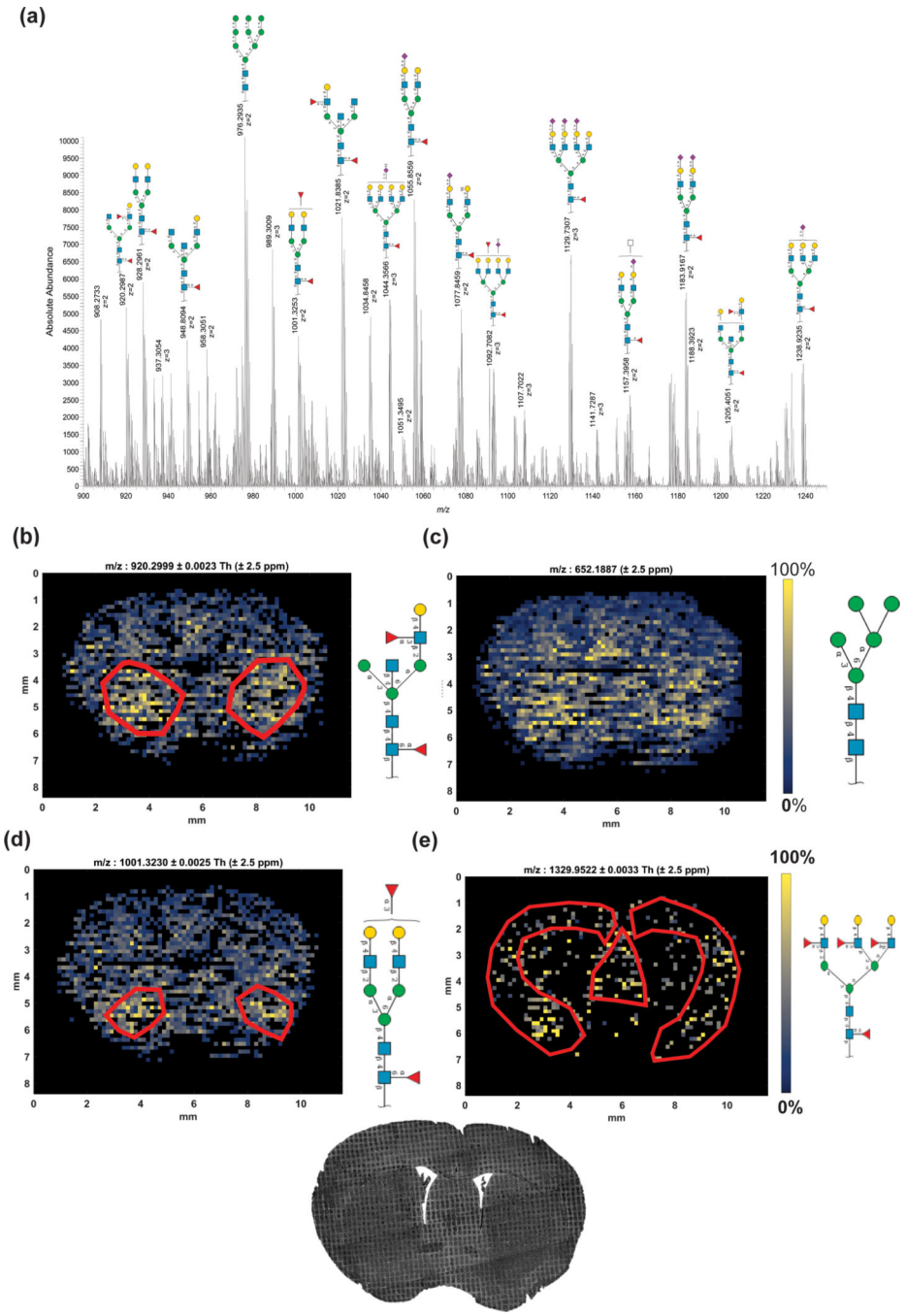

Figure 4: Spatial resolution of *N*-glycans in IR-MALDESI:

(a) Mass spectrum in the range of 900–1200 *m/z* showing a significant number of multiply-charged peaks with the annotated structures determined using GlyConnect database. Labels without the structures were the multiply-charged peaks with no GlyConnect database identifications. Colocalization with spatial features in the rodent brain (b, c, d ,e): Ion images and structures of four identified *N*-linked glycans using GlyConnect with the phase contrast image of the brain is represented to show the glycan co-localization with morphological features in the brain.

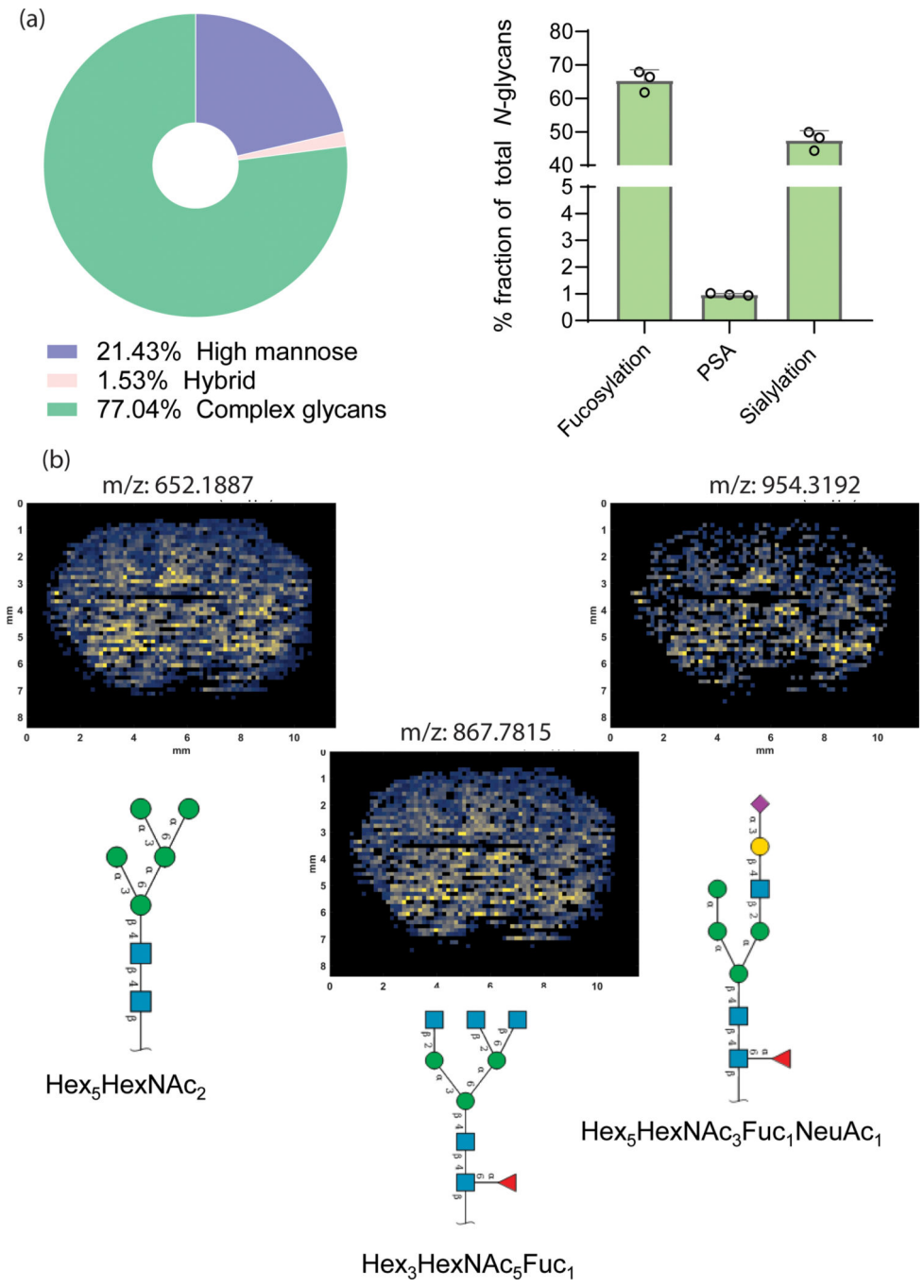

Figure 5:

Relative abundances of total *N*-glycans (a) Relative quantification of the total *N*-glycans belonging to each of the three biosynthetic classes: oligomannose, complex, and hybrid and different glycosylation traits (fucosylation, polysialylation (PSA) and overall sialylation) in the mouse brain using the IR-MALDESI, (b) Ion images of the higher abundance representative glycans from each biosynthetic class with the composition and structure identified using GlyConnect.

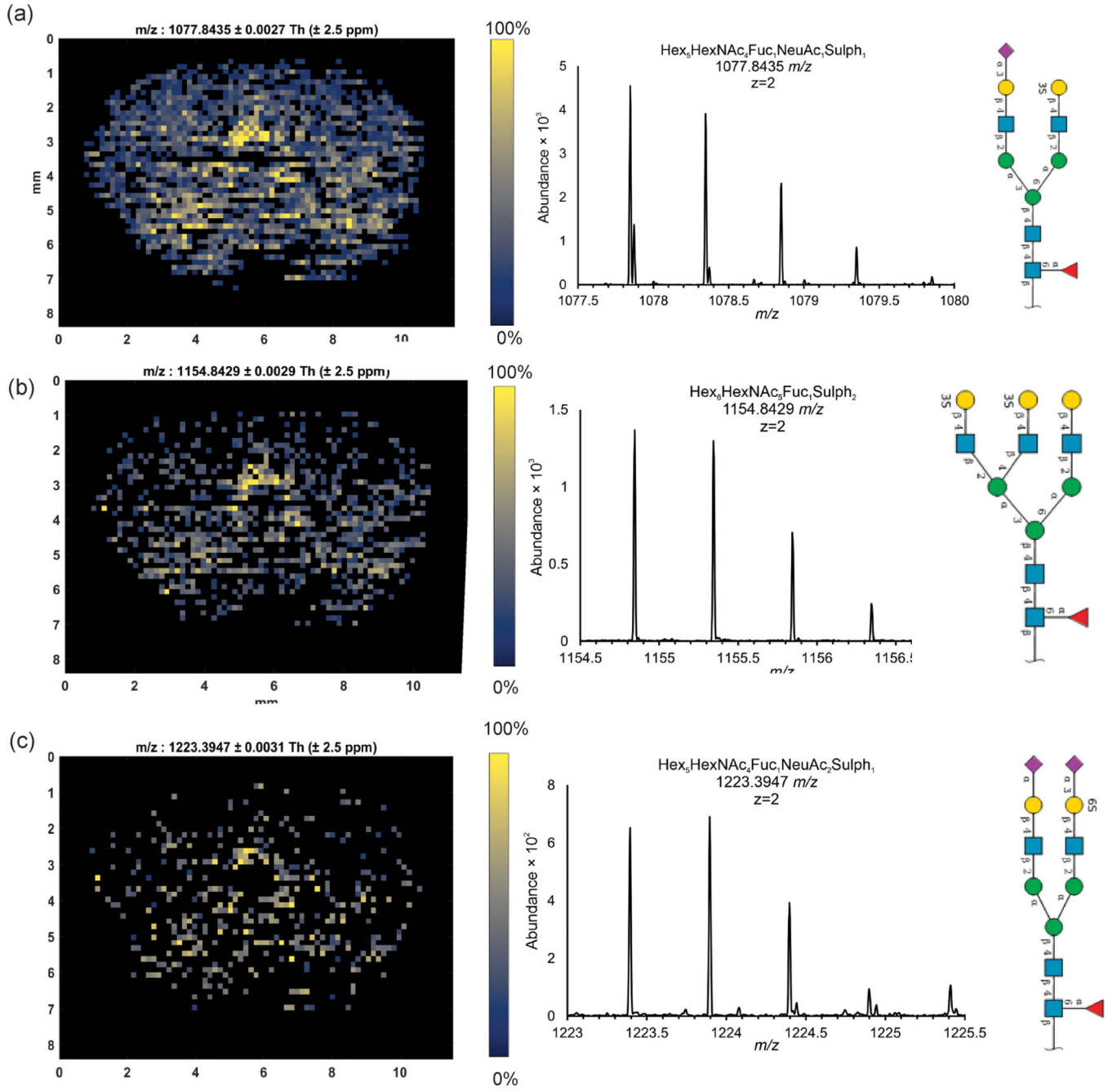

Figure 6:

Detection of sulfated brain *N*-glycans: (a, b, c) Ion images of 3 representative sulfated *N*-glycans with complete isotopic distribution for the respective charge-state (z=2) and the glycan structure and composition. The sulfated glycans show higher concentration and enhanced detected in the myelin-enriched corpus callosum.

Table 1:

Fifty most abundant multiply-charged deprotonated *N*-Linked Glycans detected in the mouse brain tissue with high mass measurement accuracy in GlyConnect. Each identification is represented in short-hand notation where H = hexose, N = N-acetylglucosamine, F = fucose, S = N-acetylneuraminic acid, Gc= *N*-glycolylneuraminic acid and Sulph = sulfate modification. (Blue: High Mannose, Green: Complex glycans; glycans arranged in the order of the abundance from high to low)

m/z	Identified *N*-glycans	Mass deviation(ppm)	*m/z*	Identified *N*-glycans	Mass deviation (ppm)
652.1870155	H5N2	1.333	1110.861362	H6N5F1	0.625
867.7821072	H3N5F1	1.108	1311.447054	H6N5F2S1	−1.372
733.2133119	H6N2	0.892	866.5887738	H6N5F1S1SULPH	−1.326
990.8219828	H5N4GC1	−0.386	826.756467	H5N3F1	2.239
766.2405952	H3N4F1	−1.472	1183.887578	H6N5F2	−1.807
976.2934079	H9N2	1.83	1329.945425	H6N5F4	−1.333
1021.837883	H4N5F2	1.239	1063.852961	H5N4F1GC1	1.55
928.2974309	H5N4F1	3.104	1293.427321	H7N6F1	0.495
855.2668314	H5N4	1.43	950.2873591	H5N4F1SULPH	3.239
895.264665	H8N2	−0.612	1077.842691	H5N4F1S1SULPH	−1.229
796.2101844	H6N5F1SULPH3	−0.064	1129.058992	H7N6F1S3	−0.517
1126.379924	H5N4GC2	0.818	1315.415566	H7N6F1SULPH	−0.983
972.2759642	H5N4F1SULPH2	1.513	1029.83528	H5N5F1	1.128
920.2993552	H4N4F2	2.454	1204.400851	H5N6F2	−1.562
948.8074241	H4N5F1	−0.302	1050.34961	H4N6F1	1.894
1001.322324	H5N4F2	−0.907	1056.688838	H9N8	3.658
847.2686836	H4N4F1	0.643	1365.977386	H6N5F1S2	−1.555
1154.842924	H6N5F1SULPH2	2.096	1548.5474	H7N6F1S2	1.241
1055.85212	H5N4F1S1	−1.662	1285.42905	H6N6F2	−0.101
1238.417731	H6N5F1S1	−1.741	1128.884343	H5N4F2S1	1.369
1420.98463	H7N6F1S1	−0.873	1092.705833	H7N6F2S2	−0.262
1256.917503	H6N5F3	−0.962	1366.455803	H7N6F2	0.092
1102.862948	H5N5F2	−0.212	902.3092718	H4N6F2	0.477
1173.385829	H6N5GC1	−2.184	959.3179993	H7N6F3	2.866
1260.412142	H3N6F1S2	−3.693	1085.334072	H7N6F1S2SULPH2	1.671